

# WISH: efficient 3D biological shape classification through Willmore flow and Spherical Harmonics decomposition

Marco Agus  
 CSE - HBKU VIC - CRS4  
 Doha, Qatar Cagliari, Italy  
 magus@hbku.edu.qa

Enrico Gobbetti  
 VIC - CRS4  
 Cagliari, Italy  
 gobbetti@crs4.it

Giovanni Pintore  
 VIC - CRS4  
 Cagliari, Italy  
 gianni@crs4.it

Corrado Calì  
 Istituto Di Neuroscienze Cavalieri Ottolenghi - UniTO  
 Torino, Italy  
 corrado.calì@unito.it

Jens Schneider  
 CSE - HBKU  
 Doha, Qatar  
 jeschneider@hbku.edu.qa

## Abstract

*Shape analysis of cell nuclei, enabled by the recent advances in nano-scale digital imaging and reconstruction methods, is emerging as a very important tool to understand low-level biological processes. Current analysis techniques, however, are performed on 2D slices or assume very simple 3D shape approximations, limiting their discrimination capabilities. In this work, we introduce a compact rotation-invariant frequency-based representation of genus-0 3D shapes represented by manifold triangle meshes, that we apply to cell nuclei envelopes reconstructed from electron micrographs. The representation is robustly obtained through Spherical Harmonics coefficients over a spherical parameterization of the input mesh obtained through Willmore flow. Our results show how our method significantly improves the state-of-the-art in the classification of nuclear envelopes of rodent brain samples. Moreover, while our method is motivated by the analysis of specific biological shapes, the framework is of general use for the compact frequency encoding of any genus-0 surface.*

## 1. Introduction

During the last decades, we witnessed the proliferation of high-throughput digital acquisition technologies capable to provide high-quality 3D representations of real-world scenes and objects in many application domains. The wide availability of massive amounts of 3D data is leading the scientific community to develop novel data-driven 3D analysis and synthesis methods. Particularly in biology and medicine, the shape analysis of cell nuclei is considered of paramount importance for computer-aided diagnostics, since size and

shape of nuclear envelopes can vary depending on cell types and other, even transient, conditions [73]. Moreover, shape analysis is also emerging as a very important tool to understand low-level biological processes. For instance, it has been shown that even little variations in nuclear shape have important impacts on the regulation of gene expression [53].

Modern nanometric-scale imaging and reconstruction techniques based on electron micrographs are starting to create collections of accurate 3D shape measurements of nuclei, making it possible to develop and exploit quantitative 3D shape analysis frameworks [7]. Geometrically, the cell nucleus has been, however, mostly studied on individual 2D images [73], or using close-to-spherical 3D structures [15, 2]. These approximations are increasingly proving themselves as substantially too coarse for a number of applications [53, 6].

In this work, we introduce a compact rotation-invariant frequency-based representation of general *genus-0* 3D shapes, represented by manifold triangle meshes that we apply to 3D reconstructions of cell nuclei envelopes (Sec. 3). To this end, natural bases, and explicitly Spherical Harmonics (SH), provide a particularly powerful tool for representing shapes in a natural way. Compact and effective rotation invariant descriptors can be obtained from SH coefficients and used for classification [29, 60].

Traditionally, the usage of SH descriptors has been limited by the fact that they are defined over a spherical domain, and deriving an efficient spherical parameterization of 3D objects is a challenging problem (Sec. 2). To overcome this issue, we apply a robust conformal parameterization based on Willmore flow [11], which makes the entire process reliable and efficient for general input shapes.

To our best knowledge, this is the first attempt to exploit

Willmore flow for shape decomposition.

We have applied our framework to the classification of digital 3D reconstructions of nuclei of brain cells obtained by segmenting serial electron micrographs at nanoscale resolution [6], demonstrating improved robustness and performance over competing techniques (see Sec. 6).

While the proposed method is motivated by a specific application in biology and medicine, our framework is of general use, and our frequency-based shape representation is readily applicable to a variety of applications, such as remeshing, analysis, on-the-fly tessellation, streaming, and classification. For example, compactness is controlled by the number of retained SH coefficients, while remeshing is easily obtained by sampling on the spherical domain.

## 2. Related work

The proposed method builds on geometry processing solutions for spherical parameterization of manifold objects, spherical harmonics decomposition, shape analysis and classification, and extends and applies them to cell nuclei analysis. Here, we only review the approaches most closely related to ours, referring readers to extensive state of the art reports for a wider overview of related fields [25, 14, 46].

**Shape analysis in neuroscience** The availability of 3D reconstructions of brain structures is driving the development of various frameworks for shape analysis in order to classify and account for variability to be associated to different structures and conditions [42, 27]. In general, shape analysis methods are targeted to the full cortex acquired with MRI methods [66]. Recent methods on 3D morphometric analysis consider frequency decomposition frameworks [58, 12], functional spaces [59], Random Markov Fields [72], or deformation maps [55, 18] and are mostly used for studying hippocampi shapes [72] or full cortices affected by Alzheimer’s disease [59]. With the emergence of high-resolution imaging data, shape analysis studies of brain structures at nanometric resolution scale are starting to appear [24, 7, 6]. In this context, Queisser et al. [53] developed a tool to retrieve the 3D view of cell nuclear envelopes from laser scanning confocal microscopy data that has been used to show how synaptic activity induces dramatic changes in the geometry of the cell nucleus [69], while Nandakumar et al. [41] applied conformal mapping to nuclear shapes obtained through optical projection tomographic microscopy. Finally, Agus et al. [1, 2] performed classification of nuclear brain cells through implicit and explicit parametric representations of cell nuclei obtained from electronic-imaging data, showing a significant improvement with respect to previous approaches based on simple spherical or ellipsoidal fittings. Here, we improve over existing work by considering a robust spherical parameterization based on conformal flow, thus resulting in

a dramatic improvement of fitting and classification accuracy for widely variable nuclear shapes.

**Shape classification** In the general 3D classification domain, the exploitation of large amounts of data by machine learning strategies has led to significant advances [8, 71]. Many current efforts attempt to work directly on raw data, be it 2D images [67, 74] or 3D voxelized representations [32, 36, 28], by designing deep neural networks in which the modelling is hidden and the feature computation and filtering of information is automatically performed by the network. In parallel, in order to simplify classification and automatic shape generation, attempts to reduce the depth of networks by introducing meaningful parameterizations or embeddings of input shapes is gaining interest, since such parameterizations can simplify the automatic classification or shape generation (model-based or “shallow” learning) and reduce the number of training examples [61]. In order to alleviate the overhead that dense voxelizations pose to deep CNNs, octrees have been proposed [67, 54]. Another option to feed 3D data into deep CNNs is the use of rendered multi-views [64, 52] or geometry images [61, 62]. While results are generally promising, Qi et al. [52] observed that convolutional neural networks (CNNs) based on multi-view renderings train slower (due to the required rendering overhead) but outperformed volumetric CNNs during inference. They address the problem with data augmentation, multi-orientation pooling and a multi-resolution approach. On an alternative route, distances [33] or moments derived from geodesic distance combined with an autoencoder [34] have been used to derive compact shape descriptors. Notably, geodesic local polar coordinates have been used [36], whereas our method uses a global parameterization. In an effort to feed scanned shapes directly into deep networks, Qi et al. designed Pointnet [51], which is invariant under point permutations in point clouds. Combinations of local features and either probabilistic Hough transforms [30] or spectral descriptors derived from the Laplace-Beltrami operator [74] have also been used to design embeddings in order to compute shape descriptors that can be fed into subsequent spatial and/or spectral CNNs. In this paper, we introduce a compact frequency-based representation that proves effective for “shallow” classification purposes. In contrast to existing work, our method relies on a compact frequency-based representation that is rotation-invariant and requires no data augmentation or pre-registration of shapes. Furthermore, since our parameterization is global and continuous, our method does not need to partition the object into local patches, disks, or derive local feature descriptors. We would also like to note that our method works with triangulated objects *as-is*, i.e., it does not require any resampling, voxelization, or rendering of multi-views. Finally, our descriptor is inherently multi-scale due to the use of Spherical Harmon-

ics and does not need explicit hierarchical data structures.

**Spherical parameterization** Geometric models are often described by closed, genus-0 surfaces. For such surfaces, there exist a homeomorphism to a sphere (that is, a continuous and invertible function that maps points from the surface to the sphere) [19, 50]. Thus, the sphere is the most natural parameterization domain, since it does not require cutting the surface into patches or disks. Spherical parameterization proves to be challenging in practice, for three reasons. Firstly, it must prevent parametric “foldovers” and thus guarantee a 1-to-1 spherical map. Secondly, while all genus-0 surfaces are topologically sphere-shaped, some can be highly deformed, and creating a parameterization that adequately samples all surface regions is difficult. Thirdly, isometric parametrizations rarely exist; the goal of conformal (preserving angles) and equiareal (preserving area) are contradicting in all but trivial cases [40]. Conformal parameterization have recently gained much interest in the computer graphics community, e.g. [31, 11], since they tend to distort textures very gracefully by preserving angles. Whereas Li et al. [31] propose to solve the Laplace-Beltrami equation using exponential maps to improve numerical robustness and complexity, more recent publications have used discrete Willmore flow [4, 44, 13]. Willmore flow is a curvature flow that can be used to smooth a 3D object into a sphere, thereby obtaining a parameterization. However, it is a fourth-order flow, which poses convergence and robustness challenges. In two successive papers, Crane et al. [10, 11] developed a computationally efficient and robust method to compute the discrete Willmore flow for triangulated meshes. In this work, we build upon their formulation for triangulated surfaces [11] to compute a conformal spherical parameterization. Non-conformal parameterizations may shear features on the model, introducing artifacts in the form of high frequency components. Such artifacts are highly undesirable for our application, since the subsequent spherical harmonics decomposition would require many more coefficients to serve as an effective shape descriptor.

**Spherical harmonics decomposition** Given a 2-manifold surface  $\mathcal{M}$ , the Laplace-Beltrami operator  $\Delta_{\mathcal{M}}$  (a directional measure of curvature) induces eigenfunctions that serve as a natural basis of functions defined over  $\mathcal{M}$ . This basis is, in general, called the *manifold harmonic basis* [65], and, in case of  $\mathcal{M}$  being a sphere, *spherical harmonics* (SH). Due to SH being the analogue of the traditional Fourier basis, it can be used to decompose functions over  $\mathcal{M}$  into frequencies. For this reason, SH have been popular in computer graphics, e.g., to precompute [20, 63] or sample [26, 38] lighting contributions. Commonly, the fact is exploited that many spherical functions occurring in natural phenomena can be approximated sufficiently using only a few SH coefficients.

SH decompositions have also been used to construct a variety of 3D shape descriptors. To obtain spherical functions, intersections between the 3D model and concentric spheres around the barycenter have been used [17, 29, 45]. General genus manifolds have been decomposed into star-shaped patches [39] to facilitate computing the spherical functions. In contrast, Li et al. [31] and our method use a conformal mapping that avoids such sampling and the associated loss of information. To this end, Li et al. solve a diffusion equation (the Laplace-Beltrami equation). To alleviate slow convergence and numerical issues, exponential maps are used. In contrast, we use a robust and computationally efficient implementation of discrete Willmore flow. To make the shape descriptor rotation-invariant, the use of SH energy invariants has been proposed [29]. Noting that energy invariants lose information, complete invariants based on canonical Euler angles and generalized Legendre polynomials have been proposed [31]. Similarly, Althlooti et al. [3] demonstrate the use of SH to robustly estimate rotation. The derived SH-based shape descriptors have been successfully used in the context of shape matching and retrieval [45, 60, 16]. In this work, we use the incomplete energy rotation invariants of Kazhdan et al. [29] for their compactness and effectiveness [60].

### 3. Method overview

Our work is motivated by the analysis of shapes representing brain structures at nanometric scale. The general workflow for 3D reconstruction consists of 3D Electron Microscopy imaging, followed by image registration, and labelling performed through manual or semi-automatic segmentation techniques [9]. Finally, surface reconstruction produces closed triangular meshes representing the different cellular structures. Given a triangle mesh representing a genus-0 surface, our framework computes a frequency-based parametrization that can be applied for classification particularly targeted to biological shapes (see Fig. 1). The method consists of three main steps:

- **spherical parameterization:** find a continuous invertible map from the unit sphere to the input mesh, which maps each mesh vertex to a sphere vertex, in a way that each mesh edge maps to a great circle arc, and each mesh triangle maps to a spherical triangle bounded by these arcs. In this work, in order to obtain a robust parameterization, we apply a fairing method based on the minimization of Willmore energy [11] (see Sec. 4).
- **spherical harmonics decomposition:** given a spherical parameterization, Spherical Harmonics provide a complete natural frequency-based basis for representing functions defined over a sphere. Given spherical functions representing the coordinates of mesh vertices, they can be represented as linear combination of harmonic functions. In this paper, we describe a least-

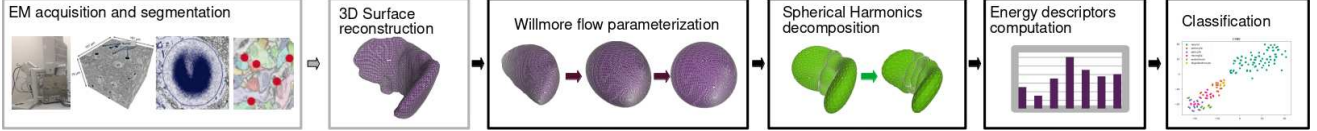


Figure 1. **Pipeline:** after acquisition and processing of biological shapes, from triangle mesh closed surfaces our framework is able to compute a frequency-based representation that is used for classification. The pipeline consists of three main steps: spherical mapping through robust discrete formulation of Willmore flow, decomposition over the spherical domain through Spherical Harmonics orthonormal basis, and shallow classification over energy descriptors.

square method for computing the coefficients of linear decomposition of coordinate functions (see Sec 5);

- **classification:** given a shape parameterization composed by a set of complex SH coefficients, energy descriptors obtained from SH coefficients [29] are used to obtain a rotation-invariant representation. These descriptions can be used to perform classification. In this work, we show how a “shallow” classification based on a Support Vector Machines applied to energy descriptors can be used to obtain state-of-the-art performance on nuclear envelope classification (see Sec 6).

Even though the proposed framework is targeted at the analysis of biological shapes, our frequency-based shape representation is of general use for a variety of applications, such as remeshing, analysis, on-the-fly tessellation, streaming, and classification.

#### 4. Willmore flow parameterization

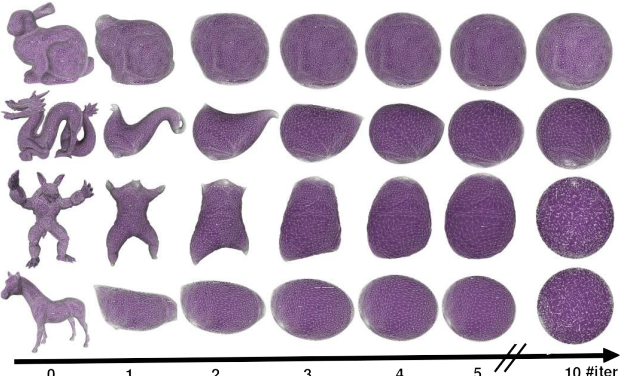


Figure 2. **Willmore flow:** Willmore flow is ideally suited to compute the spherical parameterization. A robust discrete version is able to evolve closed 2-manifolds to conformally equivalent spheres in a limited number of steps.

The goal of spherical parametrization is to find a bijective mapping from the original surface to the unit sphere. Given a genus-0 surface  $\mathcal{M}$ , a classical way to compute the mapping consists of smoothing the original shape through the minimization of Willmore energy [68], which is a measure

of how much  $\mathcal{M}$  differs from a sphere. It is defined as

$$E_W(\mathcal{M}) = \int_{\mathcal{M}} H^2 dA - \int_{\mathcal{M}} K dA, \quad (1)$$

where  $dA$  is a differential surface element,  $H$  the mean curvature and  $K$  the Gauss curvature. In this work, we are concerned with closed 2-manifolds  $\mathcal{M}$  of genus 0, for which

$$\int_{\mathcal{M}} K dA = 4\pi. \quad (2)$$

Expressing  $H = \frac{1}{2}(\kappa_1 + \kappa_2)$  and  $K = \kappa_1 \kappa_2$  in terms of principal curvatures  $\kappa_1, \kappa_2$ , the following equivalent formulation can be derived from Eq. (1).

$$E_W(\mathcal{M}) = \frac{1}{4} \int_{\mathcal{M}} (\kappa_1 - \kappa_2)^2 dA. \quad (3)$$

From this formulation, it becomes immediately obvious that the Willmore energy vanishes for a sphere ( $\kappa_1 = \kappa_2$ ), whereas it is positive otherwise.

The corresponding  $L^2$  gradient flow is called the Willmore flow. It is a particular type of curvature flow that describes the evolution of a genus-0 surface  $\mathcal{M}$  into a sphere. It is governed by the differential equation

$$\partial_t x(t) = -\nabla E_W(x(t)) \quad \forall x(t) \in \mathcal{M}. \quad (4)$$

One of the main advantages of Willmore flow is the preservation of angles (conformality), which prevents shearing of features of the mesh and avoids the introduction of unwanted high frequencies. This makes it ideally suited for a variety of applications, like texturing, remeshing, and smoothing.

In this work, we introduce Willmore flow for the first time in the context of shape analysis to compute a robust spherical parameterization for a subsequent spherical harmonics decomposition. In practice, we apply the discrete formulation proposed by Crane et al. [10, 11], which allows to develop triangulated, closed genus-0 2-manifolds to a conformally equivalent sphere in a computationally efficient fashion. Each step involves the following process: calculating smooth per-vertex normals, calculating the cotangent Laplacian using the Laplace-Beltrami operator [48], solving an eigensystem in curvature space, and a Poisson equation. From a computational perspective, despite the Willmore flow

being a fourth-order flow, all of our examples could be developed into a sphere in only 10 steps (see Fig. 2). At the end of the process, from the initial set of vertices

$$\mathbf{X} = \{ \mathbf{x}_i = (x_i, y_i, z_i) \}_{i=1}^n \subseteq \mathbb{R}^3, \quad (5)$$

we obtain the spherical map

$$\begin{aligned} \mathbf{W} : \mathbf{X} &\rightarrow S_2 \\ \mathbf{W} : \mathbf{x}_i &\mapsto \mathbf{w}_i = (\theta_i, \phi_i), \end{aligned} \quad (6)$$

where  $S_2$  denotes the unit 2-sphere embedded in  $\mathbb{R}^3$ .

## 5. Spherical Harmonics decomposition

Since we develop any genus-0 surface to a sphere through our Willmore flow parameterization, we can define any surface using spherical functions, and spherical harmonics become a natural choice to serve as basis functions [5]. They are an infinite set of complex functions that are single-valued, continuous, orthonormal, and complete on the sphere. They are defined as complex functions with respect to the order  $l$  and degree  $m$  in the following way:

$$Y_l^m(\theta, \phi) = \sqrt{\frac{2l+1}{4\pi} \frac{(l-m)!}{(l+m)!}} P_l^m(\cos \theta) e^{im\phi} \quad (7)$$

where  $l$  and  $m$  are integers such that  $|m| \leq l$ , and  $P_l^m$  are the associated Legendre polynomials [39]. In Fig. 3 the 3D graphic representations of spherical harmonics up to order  $l = 3$  are shown. Any spherical function  $f(\theta, \phi)$  can be represented by a linear combination of spherical harmonics  $Y_l^m(\theta, \phi)$  as follows:

$$f(\theta, \phi) = \sum_{l=0}^{\infty} \sum_{m=-l}^l a_l^m Y_l^m(\theta, \phi). \quad (8)$$

This spherical harmonic expansion can be interpreted as

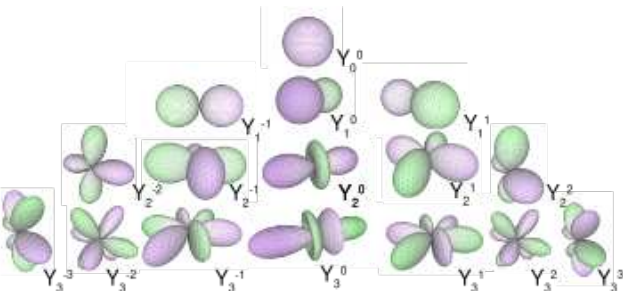


Figure 3. **Spherical harmonics:** they are complex functions depending on order  $l$  and degree  $m$ , and they represent an orthonormal basis for decomposing radial functions.

the Fourier transform for functions defined on the sphere, converting spherical scalar signals into their frequency spectrum. Spherical harmonics have several interesting properties such as orthonormality, completeness, and coarse-to-fine

hierarchy. In our case, we use them for decomposing the coordinate functions  $\mathbf{x}(\theta, \phi) = (x(\theta, \phi), y(\theta, \phi), z(\theta, \phi))$  as defined by the Willmore flow map  $\mathbf{W}$ .

For fitting, we define a vectorial surface representation  $\mathbf{x}_{L_{max}}(\theta, \phi)$  in spherical coordinates as a truncated linear combination of spherical harmonic complex components, by limiting the maximum degree to a specific value  $L_{max}$ , in a way to have a fixed number of coefficients  $k = (L_{max}+1)^2$ :

$$\mathbf{x}(\theta, \phi) \approx \mathbf{x}_{L_{max}}(\theta, \phi) = \sum_{l=0}^{L_{max}} \sum_{m=-l}^l \mathbf{c}_l^m Y_l^m(\theta, \phi), \quad (9)$$

where  $Y_l^m(\theta, \phi)$  is the harmonic function.

**Least-squares problem** The least-squares problem that we need to solve for fitting minimizes the squared distance between the points and the SH decomposition [5]. We can write equation 9 in matrix form  $\mathbf{Y}\mathbf{C}_{(x|y|z)} = \mathbf{X}_{(x|y|z)}$ , corresponding to three linear systems, one for each component:

$$\begin{bmatrix} y_{1,1} & y_{1,2} & \dots & y_{1,k} \\ y_{2,1} & y_{2,2} & \dots & y_{2,k} \\ \vdots & \vdots & \ddots & \vdots \\ y_{n,1} & y_{n,2} & \dots & y_{n,k} \end{bmatrix} \begin{bmatrix} \mathbf{c}_{1(x|y|z)} \\ \mathbf{c}_{2(x|y|z)} \\ \vdots \\ \mathbf{c}_{k(x|y|z)} \end{bmatrix} = \begin{bmatrix} \mathbf{x}_{1(x|y|z)} \\ \mathbf{x}_{2(x|y|z)} \\ \vdots \\ \mathbf{x}_{n(x|y|z)} \end{bmatrix}, \quad (10)$$

where  $y_{i,j} = Y_l^m(\mathbf{w}_i = (\theta_i, \phi_i))$ ,  $\mathbf{c}_j = \mathbf{c}_l^m$ , with  $j = l^2 + l + m + 1$ ,  $k = (L_{max}+1)^2$ , and  $\mathbf{x}_i = \mathbf{x}(\mathbf{w}_i = (\theta_i, \phi_i))$ . For smoothing the solution, we also added a Tikhonov regularization term  $\Gamma$  [22], increasingly penalizing the coefficients with increasing order  $l$ . In this way, the least square problem is defined as:

$$\mathbf{C}_{(x|y|z)} = \arg \min_{\mathbf{C}_{(x|y|z)}} \left( \|\mathbf{Y}\mathbf{C}_{(x|y|z)} - \mathbf{X}_{(x|y|z)}\|^2 + \nu \|\mathbf{\Gamma}\mathbf{C}_{(x|y|z)}\|^2 \right), \quad (11)$$

leading to the following linear systems

$$(\mathbf{Y}^H \mathbf{Y} + \nu \mathbf{R}) \mathbf{C}_{(x|y|z)} = \mathbf{Y}^H \mathbf{X}_{(x|y|z)}, \quad (12)$$

where  $\mathbf{Y}^H$  is the Hermitian (conjugate transpose) matrix of  $\mathbf{Y}$ , and where  $\mathbf{R} = \mathbf{\Gamma}^H \mathbf{\Gamma}$ :

$$\mathbf{R} = \begin{bmatrix} l_j^2(l_j^2 + 1)^2 & & 0 \\ & \ddots & \\ 0 & & l_{max}^2(l_{max}^2 + 1)^2 \end{bmatrix}. \quad (13)$$

Here,  $l_j$  is the spherical harmonics order associated with the coefficient  $j$ . In order to speed-up the decomposition process, we also considered a residual iterative fitting scheme [57]. We decomposed the fitting problem in a sum of smaller scale least square problems  $\mathbf{Y}_s \mathbf{C}_s = \mathbf{B}_s$ , such that the residual iteratively decreases ( $\mathbf{B}_s = \mathbf{X} - \mathbf{B}_{s-1}$ ). The matrix  $\mathbf{Y}_s$  is composed by separating the spherical harmonics order in bands in a way that the size of the matrix  $k_s$  does not

exceed a given threshold (in the results provided in this paper, we separated the problems to keep  $k_s = 100$ ). In all results of this paper, we used a small regularization value ( $\nu = 10^{-5}$ ). We solve the linear systems by performing a robust Cholesky decomposition with pivoting through LDLT factorization [56].

**Rotation invariance** In this work, we use the energy rotation-invariances proposed in [29, 43]. The key observation is that the  $L^2$  vector norm is preserved under rotation. Therefore, the squared norm of SH coefficients  $\mathbf{c}_l^m$  at every frequency  $l$  is independent of rotation [31]. We thus define

$$\xi(l) := \sum_{|m| \leq l} \|\mathbf{c}_l^m\|^2, \quad (14)$$

using the SH coefficients introduced in Eq. (8). While [31] points out that these invariants are incomplete—there are only  $(L_{max} + 1)$  real-valued invariants instead of  $(L_{max} + 1)^2$  complex coefficients—it is this incompleteness that make them appealing for shape classification applications [60].

## 6. Results

**Implementation notes** Our framework was implemented in C++, by using an implementation of conformal curvature flow using spin transformations (<https://github.com/nitronoid/flo>), and the Eigen library [23] for linear least-squares optimization in the case of spherical harmonics parameters. The coefficients of spherical harmonics components were found by solving the linear systems in Equation 12 (with regularization factor  $\nu = 10^{-5}$ ), and OpenMP for parallelizing the solution of linear systems over different coordinate functions. All fitting sessions were performed on a Dell XPS 8930 workstation equipped with CPU Intel i7-9700 3.0GHz, an Nvidia Geforce RTX 2060 and running Windows 10. For reconstructing the objects from an SH decomposition, we considered a recursive edge subdivision of the spherical domain, starting from icosahedron approximation of the unit sphere. We also used the parameters derived from SH decomposition for classifying the nuclei according to standard machine learning methods, that we implemented using Jupyter notebooks [21] and the scikit-learn [47] Python library.

**Dataset** Our test set is a collection of 92 3D reconstructions of brain cells nuclei. They were extracted from dense reconstructions coming from a semiautomatic segmentation of nanometric scale electron microscopy stacks, obtained after imaging a volume of brain parenchyma from layer VI somatosensory cortex of a P14 rat [6]. The nuclear shapes were manually assigned to known cell types (Fig. 4). All

considered objects are represented by triangular meshes containing around 10K vertices and 20K triangles.

**Timing and accuracy** Fig. 6 shows accuracy performance of Spherical Harmonics decomposition coupled with Willmore flow spherical mapping. For all of the considered shapes, the initial Willmore flow spherical parameterization was obtained with 10 iterations. Displacement errors computed on all shapes in Fig. 4 are reported in  $\mu\text{m}$ . As reference scale, the average diagonal of the oriented bounding boxes of the considered nuclear shapes is  $11.26 \pm 2.26 \mu\text{m}$ . Specifically, average error (Fig. 6, left) and maximum error (Fig. 6, right) are reported for increasing Spherical Harmonics decomposition (with  $L_{max}$  ranging from 5 to 25). It is evident how the fitting error monotonically decreases by increasing the number of spherical harmonics. As reference, Fig. 5 shows examples of reconstructions obtained with SH decompositions for  $L_{max}$  ranging from 5 to 25. Nuclear envelopes from different categories are presented: from top to bottom, neuron, astrocyte, endothelium, microglia, pericyte, and oligodendrocyte. It can be noted how even a limited number of coefficients ( $L_{max} = 5$ ) is able to provide a faithful approximation of the shape of nuclear envelopes.

For timing performances, in Fig. 7 we report the average computation times for the nuclear shapes on Fig. 4 with our current C++ implementation, which does not consider any kind of GPU optimization but only trivial parallel schemes provided by OpenMP. Specifically, we show the average computation time for Willmore spherical mapping left, and for SH decomposition (right). From charts, it appears evident that Willmore flow evolution is linear with respect to the number of iterations, while SH decomposition time increases with the number of coefficients, which is quadratic in  $L_{max}$ . Specifically, we obtain a total of  $(L_{max} + 1)^2$  complex coefficients per dimension, resulting (for 3D) in a total number of  $k = 6(L_{max} + 1)^2$  values.

**Classification using SVM** For using the SH parametric representation, we considered the classical support vector machine (SVM) [49, 70] with radial basis functions for deriving predictive models. To evaluate classification performance, we considered five cases for spherical harmonics parameterization with  $L_{max} = 5, 10, 15, 20, 25$  (denoted as  $SH_5, SH_{10}, SH_{15}, SH_{20}, SH_{25}$ ). To reduce the number of complex coefficients, we applied the rotation-invariant energy descriptors proposed by Kazhdan et al. [29], by computing the  $L_{max} + 1$  rotation-invariant energies  $\{\xi(l), l = 0, \dots, L_{max}\}$ , from the SH coefficients as per Eq. (14),  $\xi(l) = \sum_{m=-l}^l \|\mathbf{c}_l^m\|^2$ . For each case considered, we performed grid-searching for configuring two hyperparameters for the support vector machine model: the constant  $\gamma$  of the Gaussian radial basis function ( $K(x_i, x_j) = \exp(-\gamma \|x_i - x_j\|^2)$ ), and the weight  $C$  for

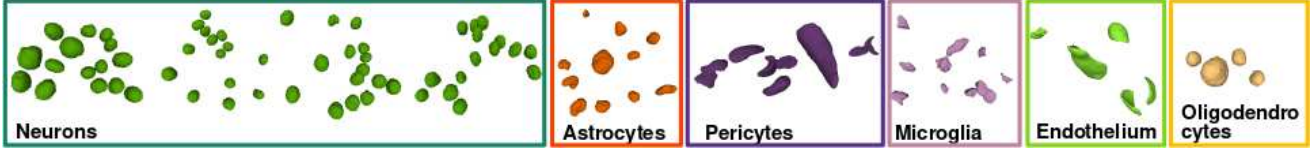


Figure 4. **Input data:** the test set is a collection of 92 3D reconstructions of brain cells nuclei: they were extracted from dense reconstructions coming from a semiautomatic segmentation of nanometric scale electron microscopy stacks, obtained after imaging a volume of brain parenchyma from layer VI somatosensory cortex of a P14 rat, and manually labelled by domain experts [6].

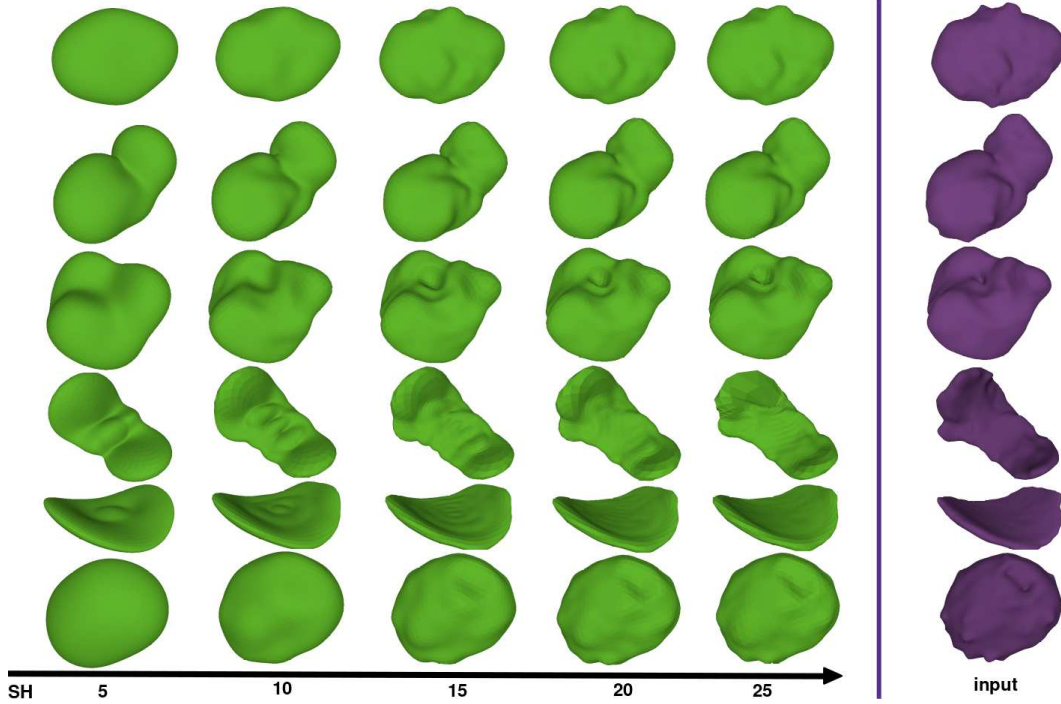


Figure 5. **Nuclear envelopes fitting accuracy:** examples of reconstruction of nuclear shapes of different classes. From top to bottom, neuron, astrocytes, endothelium, microglia, pericyte and oligodendrocyte. The reconstruction is obtained with increasing number of spherical harmonics ( $L_{max}$  ranging from 5 to 25).

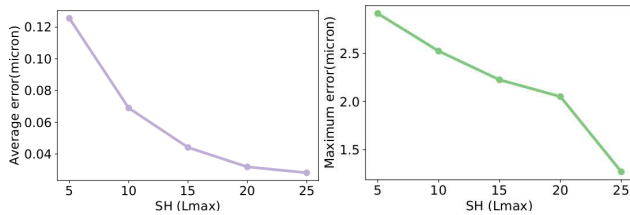


Figure 6. **Accuracy:** accuracy of SH decomposition on nuclear envelopes. For increasing number of spherical harmonics ( $L_{max}$  ranging from 5 to 25), average error (left) and maximum error (right) in  $\mu\text{m}$  are reported. As reference scale, the half diagonal of considered nuclear shapes is  $5.63 \pm 1.13 \mu\text{m}$ .

the soft margin regularization function. We carried out the model training on 92 nuclear shapes of layer VI. We performed hyperparameter optimization by using the scikit-learn StratifiedShuffleSplit cross validator, which subdivides the set in a merge of randomized stratified folds, obtained

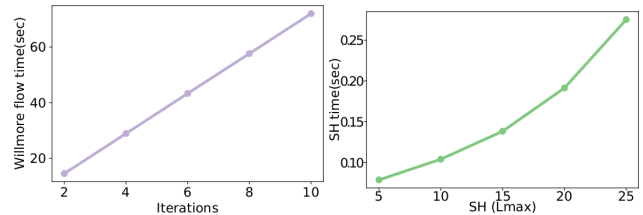


Figure 7. **Computation times:** average computation time for Willmore flow parametrization (left) and Spherical harmonics decomposition (right) are reported. Willmore flow is linear with respect to the number of iterations.

by shuffling samples in a way to preserve the percentage of samples for each class. The accuracy is evaluated with the scikit-learn on a test set that is 20% of the total set. The grid considered for hyperparameter optimization is logarithmic with  $C$  ranging from  $10^{-2}$  to  $10^{10}$ , and  $\gamma$  ranging from  $10^{-9}$  to  $10^3$ . Table 1 shows statistics of the usage of SVM

Type	Hyperp. grid	SVM params	Accuracy
$SH_5$		$\gamma = 0.01, C = 10$	0.84
$SH_{10}$		$\gamma = 10^{-3}, C = 10^3$	0.81
$SH_{15}$		$\gamma = 0.01, C = 100$	0.82
$SH_{20}$		$\gamma = 10^{-8}, C = 10^7$	0.79
$SH_{25}$		$\gamma = 10^{-3}, C = 10^5$	0.76

Table 1. **Support vector machine classification:** each representation determined specific classifier parameters during grid optimization. We show evaluation accuracies for different configurations of SVM parameters  $\gamma$  and  $C$ , the optimal set of parameters, and the corresponding evaluation accuracy.

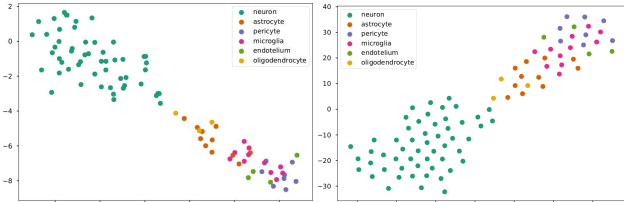


Figure 8. **t-distributed stochastic neighbor embedding:** the application of t-SNE to the invariant harmonics parametrization of nuclear envelopes confirms that there is no significant clustering difference between  $SH_5$  (left) and  $SH_{25}$  (right)

model: for each case, we show the accuracy function over the parameter grid color-mapped with ColorBrewer BuPu color scheme, the set of best SVM hyperparameters  $\gamma$  and  $C$ , and the best test accuracy score. It appears evident how even a limited number of rotation-invariant energy descriptors is able to provide accuracy above 80%, while for a big number of coefficients we start to experience overfitting. We compared the cross-correlation accuracy to results reported by Agus et al. [2], who used implicit hyperquadrics representations and SH decomposition of radial surfaces without

conformal spherical mapping. We can see how the usage of conformal Willmore flow dramatically improves the classification accuracy even for a limited number of coefficients (0.67 and 0.67 for  $SH_4$  and  $SH_{10}$  in Agus et al. [2] versus 0.84 and 0.82 for  $SH_5$  and  $SH_{10}$  for the proposed framework). This is because performing a conformal spherical allows us to gracefully handle any genus-0 shape, without degradation when significantly far from the spherical shape (see in particular endothelium, microglia, and pericyte in Fig. 5). In order to provide direct visual representation of the parameter data, we also considered classical dimension reduction schemes to have a visual representation of nuclear clusters on a reduced 2D parameter space. To this end, we used t-SNE (t-distributed stochastic neighbor embedding) [35], which maps each high-dimensional object to a two-dimensional point in such a way that similar objects are modeled by nearby points and dissimilar objects are modeled by distant points. Fig. 8 shows the results of t-SNE on spherical harmonics parameterizations  $SH_5$  and  $SH_{25}$ . Neurons (green) form a well-defined cluster which is clearly separated from all other classes, and it is evident how increasing the number of coefficients does not provide significant difference in cluster separation. Moreover, apart from a few outliers, the clusters representing the various brain cell types are clearly separated with small overlaps.

## 7. Conclusions

We presented a framework for classification of biological shapes represented by manifold genus-0 closed surfaces. Our approach is based on conformal spherical mapping through Willmore flow, followed by frequency-based decomposition through Spherical Harmonics. We tested the method on the classification of a set of nanoscale reconstructions of brain cells nuclear envelopes of a juvenile rat, demonstrating the capability to capture the overall shape with few coefficients, and achieving state-of-the art results in the classification task. The obtained representation is compact and meaningful, and it can be extended in various ways: first of all, for the analysis of more complicated shapes exhibiting higher frequency details, we plan to reduce the computation complexity of SH decomposition by combining incremental schemes based on the sampling theorems over spherical domain [37] with local density representations induced by conformal mapping over the sphere. Moreover, we plan to exploit our Spherical Harmonics decomposition framework for evaluating other rotation-invariant representations, like distance to barycenter, curvature, or histograms, for shallow classification, as well as for embedding for feeding deep classifiers for more general shape analysis tasks on heterogeneous shape collections.

**Acknowledgments.** We acknowledge the contribution of Sardinian Regional Authorities under project VIGECLAB. We thank Helmut Pottmann (TU Wien) for the useful comments and suggestions.

## References

- [1] Marco Agus, C. Cali, A. Tapia Morales, H.O. Levaslaiho, Pierre Magistretti, Enrico Gobbetti, and Markus Hadwiger. Hyperquadrics for shape analysis of 3D nanoscale reconstructions of brain cell nuclear envelopes. In *Proc. Smart Tools and Apps for Graphics*, pages 115–122, October 2018. [2](#)
- [2] Marco Agus, Maria Veloz Castillo, Javier F. Garnica Molina, Enrico Gobbetti, Heikki Levaslaiho, Alex Morales Tapia, Pierre Magistretti, Markus Hadwiger, and Corrado Calí. Shape analysis of 3d nanoscale reconstructions of brain cell nuclear envelopes by implicit and explicit parametric representations. *Computers & Graphics*, 2019. [1](#), [2](#), [8](#)
- [3] Salah Althoothi, Mohammad H Mahoor, and Richard M Voyles. A robust method for rotation estimation using spherical harmonics representation. *IEEE TIP*, 22(6):2306–2316, 2013. [3](#)
- [4] Alexander I Bobenko and Peter Schröder. Discrete Willmore flow. In *Proc. SGP*, pages 101–110, 2005. [3](#)
- [5] Ch Brechbühler, Guido Gerig, and Olaf Kübler. Parametrization of closed surfaces for 3-D shape description. *Proc. CVPR*, 61(2):154–170, 1995. [5](#)
- [6] Corrado Calí, Marco Agus, Kalpana Kare, Daniya Boges, Heikki Levaslaiho, Markus Hadwiger, and Pierre Magistretti. 3D cellular reconstruction of cortical glia and parenchymal morphometric analysis from serial block-face electron microscopy of juvenile rat. *Progress in Neurobiology*, page 101696, 09 2019. [1](#), [2](#), [6](#), [7](#)
- [7] Corrado Calí, Jumana Baghabra, Daniya J Boges, Glendon R Holst, Anna Kreshuk, Fred A Hamprecht, Madhusudhanan Srinivasan, Heikki Levaslaiho, and Pierre J Magistretti. Three-dimensional immersive virtual reality for studying cellular compartments in 3d models from em preparations of neural tissues. *J. of Comp. Neurology*, 524(1):23–38, 2016. [1](#), [2](#)
- [8] Angel X Chang, Thomas Funkhouser, Leonidas Guibas, Pat Hanrahan, Qixing Huang, Zimo Li, Silvio Savarese, Manolis Savva, Shuran Song, Hao Su, et al. Shapenet: An information-rich 3d model repository. *arXiv preprint arXiv:1512.03012*, 2015. [2](#)
- [9] Jay S Coggan, Corrado Calí, Daniel Keller, Marco Agus, Daniya Boges, Marwan Abdellah, Kalpana Kare, Heikki Levaslaiho, Stefan Eilemann, Renaud Blaise Jolivet, et al. A process for digitizing and simulating biologically realistic oligocellular networks demonstrated for the neuro-glio-vascular ensemble. *Frontiers in neuroscience*, 12, 2018. [3](#)
- [10] Keenan Crane, Ulrich Pinkall, and Peter Schröder. Spin transformations of discrete surfaces. *ACM TOG*, 30(4):104:1–104:10, 2011. [3](#), [4](#)
- [11] Keenan Crane, Ulrich Pinkall, and Peter Schröder. Robust fairing via conformal curvature flow. *ACM TOG*, 32(4):61:1–61:10, 2013. [1](#), [3](#), [4](#)
- [12] Christel Ducroz, Jean-Christophe Olivo-Marin, and Alexandre Dufour. Characterization of cell shape and deformation in 3d using spherical harmonics. In *Proc. ISBI*, pages 848–851, 2012. [2](#)
- [13] Gerhard Dziuk. Computational parametric Willmore flow. *Numerische Mathematik*, 111(1):55, 2008. [3](#)
- [14] Michael S Floater and Kai Hormann. Surface parameterization: a tutorial and survey. In *Advances in multiresolution for geometric modelling*, pages 157–186. Springer, 2005. [2](#)
- [15] M. Fricker, M. Hollinshead, N. White, and D. Vaux. Interphase nuclei of many mammalian cell types contain deep, dynamic, tubular membrane-bound invaginations of the nuclear envelope. *Cell Biology*, 136(3):531–544, 1997. [1](#)
- [16] Thomas Funkhouser, Patrick Min, Michael Kazhdan, Joyce Chen, Alex Halderman, David Dobkin, and David Jacobs. A search engine for 3d models. *ACM TOG*, 22(1):83–105, 2003. [3](#)
- [17] Guido Gerig, Martin Styner, D Jones, Daniel Weinberger, and Jeffrey Lieberman. Shape analysis of brain ventricles using spharm. In *Proc. MMBIA*, pages 171–178, 2001. [3](#)
- [18] E Gladilin, S Goetze, J Mateos-Langerak, R Van Driel, Roland Eils, and K Rohr. Shape normalization of 3d cell nuclei using elastic spherical mapping. *Journal of microscopy*, 231(1):105–114, 2008. [2](#)
- [19] Craig Gotsman, Craig Gotsman, Xianfeng Gu, and Alla Sheffer. Fundamentals of spherical parameterization for 3d meshes. *ACM TOG*, 22(3):358–363, 2003. [3](#)
- [20] Robin Green. Spherical harmonic lighting: The gritty details. In *Archives of the Game Developers Conference*, volume 56, page 4, 2003. [3](#)
- [21] Björn A Grüning, Eric Rasche, Boris Rebollo-Jaramillo, Carl Eberhard, Torsten Houwaart, John Chilton, Nate Coraor, Rolf Backofen, James Taylor, and Anton Nekrutenko. Jupyter and galaxy: Easing entry barriers into complex data analyses for biomedical researchers. *PLoS computational biology*, 13(5):e1005425, 2017. [6](#)
- [22] André F. R. Guarda, José M. Bioucas-Dias, Nuno M. M. Rodrigues, and Fernando Pereira. Improving point cloud to surface reconstruction with generalized tikhonov regularization. In *Proc. IEEE MMSP*, 2017. [5](#)
- [23] Gaël Guennebaud, Benoit Jacob, Philip Avery, Abraham Bachrach, Sébastien Barthelemy, et al. Eigen. [eigen.tuxfamily.org](http://eigen.tuxfamily.org), 2010. [6](#)
- [24] S Härtel, J Jara, CG Lemus, and ML Concha. 3d morphotopological analysis of asymmetric neuronal morphogenesis in developing zebrafish. *Computational modelling of objects represented in images. Fundamentals, methods and applications*, 6:215–220, 2018. [2](#)
- [25] Kai Hormann, Konrad Polthier, and Alla Sheffer. Mesh parameterization: Theory and practice. In *ACM SIGGRAPH ASIA 2008 Courses*, pages 12:1–12:87, 2008. [2](#)
- [26] Wojciech Jarosz, Nathan A Carr, and Henrik Wann Jensen. Importance sampling spherical harmonics. *Computer Graphics Forum*, 28(2):577–586, 2009. [3](#)
- [27] Alexandre A Kalinin, Ari Allyn-Feuer, Alex Ade, Gordon-Victor Fon, Walter Meixner, David Dilworth, Syed S Husain, Jeffrey R de Wett, Gerald A Higgins, Gen Zheng, et al. 3D shape modeling for cell nuclear morphological analysis and classification. *Scientific reports*, 8, 2018. [2](#)
- [28] Hiroharu Kato, Yoshitaka Ushiku, and Tatsuya Harada. Neural 3d mesh renderer. In *Proc. CPVR*, pages 3907–3916, 2018. [2](#)

[29] Michael Kazhdan, Thomas Funkhouser, and Szymon Rusinkiewicz. Rotation invariant spherical harmonic representation of 3D shape descriptors. In *Proc. SGP*, pages 156–164, 2003. 1, 3, 4, 6

[30] Jan Knopp, Mukta Prasad, Geert Willems, Radu Timofte, and Luc Van Gool. Hough transform and 3D SURF for robust three dimensional classification. In *Proc. ECCV*, pages 589–602, 2010. 2

[31] Hongdong Li and Richard Hartley. Conformal spherical representation of 3D genus-zero meshes. *Pattern Recognition*, 40(10):2742–2753, 2007. 3, 6

[32] Jun Li, Kai Xu, Siddhartha Chaudhuri, Ersin Yumer, Hao Zhang, and Leonidas Guibas. Grass: Generative recursive autoencoders for shape structures. *ACM TOG*, 36(4):52, 2017. 2

[33] Haibin Ling and David W Jacobs. Shape classification using the inner-distance. *IEEE TPAMI*, 29(2):286–299, 2007. 2

[34] Lorenzo Luciano and A Ben Hamza. Deep learning with geodesic moments for 3D shape classification. *Pattern Recognition Letters*, 105:182–190, 2018. 2

[35] Laurens van der Maaten and Geoffrey Hinton. Visualizing data using t-sne. *Journal of machine learning research*, 9(Nov):2579–2605, 2008. 8

[36] Jonathan Masci, Davide Boscaini, Michael Bronstein, and Pierre Vandergheynst. Geodesic convolutional neural networks on riemannian manifolds. In *Proc. ICCV workshops*, pages 37–45, 2015. 2

[37] Jason D McEwen, Gilles Puy, Jean-Philippe Thiran, Pierre Vandergheynst, Dimitri Van De Ville, and Yves Wiaux. Sampling theorems and compressive sensing on the sphere. In *Wavelets and Sparsity XIV*, volume 8138, page 81381F. International Society for Optics and Photonics, 2011. 8

[38] Jonathan T Moon, Bruce Walter, and Steve Marschner. Efficient multiple scattering in hair using spherical harmonics. *ACM TOG*, 27(3):31, 2008. 3

[39] M-H Mousa, Raphaëlle Chaine, Samir Akkouche, and Eric Galin. Toward an efficient triangle-based spherical harmonics representation of 3d objects. *Computer Aided Geometric Design*, 25(8):561–575, 2008. 3, 5

[40] Saad Nadeem, Zhengyu Su, Wei Zeng, Arie Kaufman, and Xianfeng Gu. Spherical parameterization balancing angle and area distortions. *IEEE TVCG*, 23(6):1663–1676, 2016. 3

[41] Vivek Nandakumar, Xing An, Yalin Wang, Roger Johnson, and Deirdre Meldrum. Conformal mapping of nuclei in 3d tomographic cell images to assess shape heterogeneity. In *2012 9th IEEE International Symposium on Biomedical Imaging (ISBI)*, pages 222–225. IEEE, 2012. 2

[42] Bernard Ng, Matthew Toews, Stanley Durrleman, and Yonggang Shi. Shape analysis for brain structures. In *Shape Analysis in Medical Image Analysis*, pages 3–49, 2014. 2

[43] Marcin Novotni and Reinhard Klein. Zernike descriptors for content based shape retrieval. In *Proc. ACM Solid Modeling and Applications*, pages 215–225, 2003. 6

[44] Nadine Olschläger and Martin Rumpf. Two step time discretization of Willmore flow. In *Proc. IMA Int. Conf. on Mathematics of Surfaces*, pages 278–292, 2009. 3

[45] Panagiotis Papadakis, Ioannis Pratikakis, Stavros Perantonis, and Theoharis Theoharis. Efficient 3D shape matching and retrieval using a concrete radialized spherical projection representation. *Pattern Recognition*, 40(9):2437–2452, 2007. 3

[46] Giuseppe Patané. STAR-Laplacian spectral kernels and distances for geometry processing and shape analysis. *Computer Graphics Forum*, 35(2):599–624, 2016. 2

[47] Fabian Pedregosa, Gaël Varoquaux, Alexandre Gramfort, Vincent Michel, Bertrand Thirion, Olivier Grisel, Mathieu Blondel, Peter Prettenhofer, Ron Weiss, Vincent Dubourg, et al. Scikit-learn: Machine learning in python. *Journal of machine learning research*, 12(Oct):2825–2830, 2011. 6

[48] Ulrich Pinkall and Konrad Polthier. Computing discrete minimal surfaces and their conjugates. *Experimental Mathematics*, 2:15–36, 1993. 4

[49] John Platt et al. Probabilistic outputs for support vector machines and comparisons to regularized likelihood methods. *Advances in large margin classifiers*, 10(3):61–74, 1999. 6

[50] Emil Praun and Hugues Hoppe. Spherical parametrization and remeshing. *ACM TOG*, 22(3):340–349, 2003. 3

[51] Charles R Qi, Hao Su, Kaichun Mo, and Leonidas J Guibas. Pointnet: Deep learning on point sets for 3d classification and segmentation. In *Proc. CVPR*, pages 652–660, 2017. 2

[52] Charles R Qi, Hao Su, Matthias Nießner, Angela Dai, Mengyuan Yan, and Leonidas J Guibas. Volumetric and multi-view cnns for object classification on 3d data. In *Proc. CVPR*, pages 5648–5656, 2016. 2

[53] Sean Gillian Queisser, Malte Wittmann, Hilmar Bading, and Gabriel Wittum. Filtering, reconstruction, and measurement of the geometry of nuclei from hippocampal neurons based on confocal microscopy data. *Journal of Biomedical Optics*, 13(1):014009, 2008. 1, 2

[54] Gernot Riegler, Ali Osman Ulusoy, and Andreas Geiger. Octnet: Learning deep 3d representations at high resolutions. In *Proc. CVPR*, pages 3577–3586, 2017. 2

[55] Gustavo K Rohde, Alexandre JS Ribeiro, Kris N Dahl, and Robert F Murphy. Deformation-based nuclear morphometry: Capturing nuclear shape variation in hela cells. *Cytometry Part A: The Journal of the International Society for Analytical Cytology*, 73(4):341–350, 2008. 2

[56] Michael A Saunders et al. Cholesky-based methods for sparse least squares: The benefits of regularization. *Linear and nonlinear conjugate gradient-related methods*, 100:92–100, 1996. 6

[57] Li Shen and Moo K Chung. Large-scale modeling of parametric surfaces using spherical harmonics. In *Third International Symposium on 3D Data Processing, Visualization, and Transmission (3DPVT'06)*, pages 294–301. IEEE, 2006. 5

[58] Li Shen, Hany Farid, and Mark A McPeek. Modeling three-dimensional morphological structures using spherical harmonics. *Evolution: International Journal of Organic Evolution*, 63(4):1003–1016, 2009. 2

[59] Jie Shi, Wen Zhang, and Yalin Wang. Shape analysis with hyperbolic wasserstein distance. In *Proc. CVPR*, pages 5051–5061, 2016. 2

[60] P. Shilane, P. Min, M. Kazhdan, and T. Funkhouser. The Princeton shape benchmark. In *Shape Modeling International*, pages 167–178, 2004. 1, 3, 6

[61] Ayan Sinha, Jing Bai, and Karthik Ramani. Deep learning 3D shape surfaces using geometry images. In *Proc. ECCV*, pages 223–240. Springer, 2016. 2

[62] Ayan Sinha, Asim Unmesh, Qixing Huang, and Karthik Ramani. Surfnet: Generating 3d shape surfaces using deep residual networks. In *Proc. CVPR*, pages 6040–6049, 2017. 2

[63] Peter-Pike Sloan. Stupid spherical harmonics (sh) tricks. In *Game developers conference*, pages 1–42, 2008. 3

[64] Hang Su, Subhransu Maji, Evangelos Kalogerakis, and Erik Learned-Miller. Multi-view convolutional neural networks for 3d shape recognition. In *Proc. ICCV*, pages 945–953, 2015. 2

[65] Bruno Vallet and Bruno Lévy. Spectral geometry processing with manifold harmonics. *Computer Graphics Forum*, 27(2):251–260, 2008. 3

[66] Christian Wachinger, Polina Golland, William Kremen, Bruce Fischl, Martin Reuter, et al. Brainprint: A discriminative characterization of brain morphology. *NeuroImage*, 109:232–248, 2015. 2

[67] Peng-Shuai Wang, Yang Liu, Yu-Xiao Guo, Chun-Yu Sun, and Xin Tong. O-cnn: Octree-based convolutional neural networks for 3d shape analysis. *ACM TOG*, 36(4):72, 2017. 2

[68] T.J. Willmore. A survey on Willmore immersions. In *Geometry and Topology of Submanifolds IV*, pages 11–16, 1992. 4

[69] Malte Wittmann, Gillian Queisser, Anja Eder, J Simon Wiegert, C Peter Bengtson, Andrea Hellwig, Gabriel Wittum, and Hilmar Bading. Synaptic activity induces dramatic changes in the geom. of the cell nucleus: interplay between nuclear structure, histone h3 phosphorylation, and nuclear calcium signaling. *Journ. of Neurosc.*, 29(47):14687–14700, 2009. 2

[70] Ting-Fan Wu, Chih-Jen Lin, and Ruby C. Weng. Probability estimates for multi-class classification by pairwise coupling. *J. Mach. Learn. Res.*, 5:975–1005, Dec. 2004. 6

[71] Zhirong Wu, Shuran Song, Aditya Khosla, Fisher Yu, Lin-guang Zhang, Xiaoou Tang, and Jianxiong Xiao. 3d shapenets: A deep representation for volumetric shapes. In *Proc. CVPR*, pages 1912–1920, 2015. 2

[72] Pengdong Xiao, Nick Barnes, and Tiberio Caetano. 3-d shape matching and non-rigid correspondence for hippocampi based on markov random fields. *IEEE TIP*, 27(3):1271–1281, 2018. 2

[73] Fuyong Xing and Lin Yang. Robust nucleus/cell detection and segmentation in digital pathology and microscopy images: a comprehensive review. *IEEE reviews in biomedical engineering*, 9:234–263, 2016. 1

[74] Li Yi, Hao Su, Xingwen Guo, and Leonidas J Guibas. Syncspeccnn: Synchronized spectral cnn for 3d shape segmentation. In *Proc. CVPR*, pages 2282–2290, 2017. 2